frontiers in Neuroanatomy

ORIGINAL RESEARCH
published: 30 April 2019
doi: 10.3389/fnana.2019.00045

Distribution Patterns of Three Molecularly Defined Classes of GABAergic Neurons Across Columnar Compartments in Mouse Barrel Cortex

*Zsuzsanna Almási[1], Csaba Dávid[1], Mirko Witte[2] and Jochen F. Staiger[2]**

[1] Department of Anatomy, Histology and Embryology, Semmelweis University, Budapest, Hungary, [2] Center Anatomy, Institute for Neuroanatomy, Georg-August-University Göttingen, Göttingen, Germany

The mouse somatosensory cortex is an excellent model to study the structural basis of cortical information processing, since it possesses anatomically recognizable domains that receive different thalamic inputs, which indicates spatial segregation of different processing tasks. In this work we examined three genetically labeled, non-overlapping subpopulations of GABAergic neurons: parvalbumin- (PV+), somatostatin- (SST+), and vasoactive intestinal polypeptide-expressing (VIP+) cells. Each of these subpopulations displayed a unique cellular distribution pattern across layers. In terms of columnar localization, the distribution of these three populations was not quantitatively different between barrel-related versus septal compartments in most layers. However, in layer IV (LIV), SST+, and VIP+, but not PV+ neurons preferred the septal compartment over barrels. The examined cell types showed a tendency toward differential distribution in supragranular and infragranular barrel-related versus septal compartments, too. Our data suggests that the location of GABAergic neuron cell bodies correlates with the spatial pattern of cortical domains receiving different kinds of thalamic input. Thus, at least in LIV, lemniscal inputs present a close spatial relation preferentially to PV+ cells whereas paralemniscal inputs target compartments in which more SST+ and VIP+ cells are localized. Our findings suggest pathway-specific roles for neocortical GABAergic neurons.

Keywords: barrel cortex, GABAergic neuron, parvalbumin, somatostatin, vasoactive intestinal peptide (VIP), cortical laminae, septa

OPEN ACCESS

Edited by:
Kathleen S. Rockland, Boston University, United States

Reviewed by:
Joshua C. Brumberg, Queens College (CUNY), United States
Akiya Watakabe, RIKEN Center for Brain Science (CBS), Japan

****Correspondence:***
Jochen F. Staiger
jochen.staiger@med.uni-goettingen.de

Received: *21 January 2019*
Accepted: *02 April 2019*
Published: *30 April 2019*

Citation:
Almási Z, Dávid C, Witte M and Staiger JF (2019) Distribution Patterns of Three Molecularly Defined Classes of GABAergic Neurons Across Columnar Compartments in Mouse Barrel Cortex. Front. Neuroanat. 13:45. doi: 10.3389/fnana.2019.00045

INTRODUCTION

The neocortex contains two main groups of neurons: the excitatory glutamatergic cells and the inhibitory GABAergic cells, which both are crucial for sensory information processing (Harris and Mrsic-Flogel, 2013). These two groups are molecularly, morphologically and physiologically distinct. Excitatory pyramidal cells make up approximately 80–90% of all neocortical cells and can be grouped according to laminar location and projection targets (Huang, 2014; Harris and Shepherd, 2015). Inhibitory GABAergic neurons comprise only about 10–20% of the total

population of neocortical neurons, but their diversity is surprisingly large (Markram et al., 2004; Rudy et al., 2011; De Felipe et al., 2013; Tremblay et al., 2016; Feldmeyer et al., 2018). The parvalbumin (PV+), somatostatin (SST+), and vasoactive intestinal polypeptide (VIP+) expressing cells account for the majority of GABAergic neurons (roughly 40% PV, 30% SST, and 10–15% VIP). These three distinct classes show minimal overlap in all examined cortical areas (Pfeffer et al., 2013; Tremblay et al., 2016), and have diverse molecular, structural and electrophysiological features. However, their detailed distribution and specific functions are largely unknown. A non-uniform distribution would imply distinct functions in local circuits of the barrel cortex (Feldmeyer et al., 2013). In this frame, we described the spatial distribution of these neuron types, in order to investigate their relationship to cortical compartments receiving different thalamic afferentation.

Sensory information from the whisker pad is transmitted via modularly organized parallel pathways to the barrel cortex (Diamond et al., 2008; Feldmeyer et al., 2013; Zembrzycki et al., 2013). The trigeminal nerve projects to several nuclei in the brainstem, namely the mesencephalic, principal (or pontine) and spinal nucleus. The lemniscal pathway originates in the principal trigeminal nucleus and relays tactile information via the barreloids of the ventral posteromedial nucleus (VPM) of the thalamus. The paralemniscal pathway routes its information through the spinal trigeminal nucleus (intermediate part) and medial part of the posterior thalamic nucleus (POm). From thalamus, ascending information reaches different cortical areas and layers. The primary site of termination is the barrel cortex, where the lemniscal thalamocortical fibers strongly project to layer IV (LIV) and thus also define supragranular and infragranular compartments, which are radially aligned with a barrel (Woolsey and van der Loos, 1970). This leads to the formation of barrel-related columns that are driven by their corresponding whiskers (Staiger et al., 2002; Wagener et al., 2016). Barrel columns are separated by septal compartments (Kim and Ebner, 1999; Alloway et al., 2004). The lemniscal pathway projects via VPM to the barrel columns, most strongly into LIV, layer Vb (LVb), layer VI (LVI), and less strongly to layer II/III (LII/III) (Lu and Lin, 1993; Bureau et al., 2006; Oberlaender et al., 2012), whereas the paralemniscal pathway projects via POm preferentially to layer I (LI) and layer Va (LVa) in a column-overarching manner and sends a few fibers to the LIV septum (Alloway, 2008; Wimmer et al., 2010b).

Single-cell recordings *in vivo* and *in vitro*, combined with biocytin filling and morphological reconstruction, revealed functional and morphological features of the different GABAergic neurons, found in the three subpopulations (Markram et al., 2004; Jiang et al., 2015; Tremblay et al., 2016; Feldmeyer et al., 2018). PV+ cells are located in all cortical layers (but LI). They prefer layers IV and Vb, however (Celio, 1986). Their dendritic and axonal arbors can show diverse patterns, depending on the precise laminar location of the soma; in this home layer the densest axonal as well as dendritic arborization can be found (Wang et al., 2002; Munoz et al., 2014; Koelbl et al., 2015). Their inhibitory influence strongly affects their own population (Tamas et al., 2000; Staiger et al., 2009; Pfeffer et al., 2013), but they can effectively inhibit other GABAergic interneuron types (David et al., 2007; Jiang et al., 2015; Karnani et al., 2016b; Walker et al., 2016). Furthermore, they are classically considered to be (together with the rare axo-axonic cell) the most effective inhibitors of pyramidal cells (Kubota et al., 2015; Neske et al., 2015).

SST+ cells show a bias toward infragranular layers. However, the different subpopulations, namely Martinotti and non-Martinotti cells, can show very distinct patterns of soma localization and axonal targeting (Oliva et al., 2000; Ma et al., 2006; Urban-Ciecko and Barth, 2016; Nigro et al., 2018). Compared to PV+ cells, they rather seem to avoid inhibiting other SST+ cells, but impose strong inhibition on other interneurons and pyramidal cells, in a cell type-specific manner (Caputi et al., 2009; Pfeffer et al., 2013; Xu et al., 2013). To exert their likely distal dendritic inhibition, they send dense axonal projections strongly but not exclusively into LI whereas their dendritic arborization is far less wide-ranging but usually not restricted to the home layer (Ma et al., 2006; McGarry et al., 2010; Nigro et al., 2018).

By contrast, VIP+ cells show a preferential location in the supragranular layers of mouse and rat barrel cortex (Bayraktar et al., 2000; Prönneke et al., 2015) and have recently been implicated in parallel disinhibitory and inhibitory circuits, impinging on pyramidal cells (Lee et al., 2013; Pi et al., 2013; Garcia-Junco-Clemente et al., 2017; Kuchibhotla et al., 2017; Zhou et al., 2017). In terms of input-output patterns, we have recently suggested that L II/III VIP+ cells have a dendritic tree that is largely restricted to L I-III but an axonal arbor that reaches all layers of a barrel-related column. On the other hand, VIP+ neurons in L IV-VI display a variable dendritic tree that could span all layers, whereas the axon is basically confined to infragranular layers (Prönneke et al., 2015). A major connectivity motif is VIP+ cells inhibiting SST+ Martinotti cells, in barrel as well as visual cortex (Caputi et al., 2009; Pfeffer et al., 2013; Karnani et al., 2016a; Walker et al., 2016).

As already noted above, thalamocortical projections and interneuron somata show layer preferences. However, there are also columns as another organizational principle of the cortex (Mountcastle, 1997). Although a barrel-related column preference of lemniscal and a septal compartment (often also called column) preference of paralemniscal thalamocortical fibers are well described, there is very little information available about the barrel- or septum-related columnar preferences of GABAergic neurons. There are only few cases, where not only the laminar, but the horizontal distribution was examined (Hajós et al., 1998; Nogueira-Campos et al., 2012). It is known that different types of interneurons can be the target of thalamocortical fibers of different origin (Staiger et al., 1996a,b; Porter et al., 2001; Cruikshank et al., 2010; Ji et al., 2016; Audette et al., 2017; Maffei, 2017). However, a more refined knowledge on the distribution pattern could help design experiments to further analyze thalamic inputs to GABAergic neurons in more detail.

Thus, in the present study, we aimed to answer the question whether PV+, SST+, and VIP+ neurons show a preference for the laminar and columnar compartments of the barrel cortex, as defined by the two main thalamocortical pathways.

Since LIV has a unique and central role as an access point of tactile information to the cortex and the barrel versus septum distinction is most obvious there, we put a special focus on this layer. The main question thus was, whether a compartment-associated distribution of GABAergic neurons can be found? Our results show that although laminar and columnar preferences obviously do exist for the soma locations of PV+, SST+, and VIP+ cells, only in LIV and only for SST+ and VIP+ cells, these differences reach statistical significance.

MATERIALS AND METHODS

Animals

Three different genetically engineered mouse strains were used for the present experiments: (1) a cross breed of PVcre/tdTomato mice (crossed B6;129P2-Pvalbtm1(cre)Arbr/J with B6.Cg-Gt(ROSA)26Sortm9(CAG-tdTomato)Hze/J mice) and GIN (Oliva et al., 2000) mice (PV-GIN; n = 6, male), which expressed the red fluorescent protein tdTomato in PV cells and green fluorescent protein (GFP) in a subset of SST cells, (2) SSTcre/tdTomato mice (crossed Ssttm2.1(cre)Zjh/J with B6.Cg-Gt(ROSA)26Sortm9(CAG-tdTomato)Hze/J mice) (n = 7, male) were used for visualizing all somatostatin cells, and (3) VIPcre/tdTomato mice (crossed VIPtm1(cre)Zjh with B6.Cg-Gt(ROSA)26Sortm9(CAG-tdTomato)Hze/J mice) (n = 9, male), were used to label all vasoactive intestinal polypeptide (VIP) cells. The age of animals was between 6 and 8 weeks. All used animals were obtained from the breeding facility of the University Medical Center Göttingen (Germany). Animal numbers and their suffering were restricted to the minimum. This study was carried out in accordance with the principles of the Basel Declaration and German laws on animal research (TierSchG and TierSchVersV, 2013). The protocol was approved by the LAVES (Niedersächsisches Landesamt für Verbraucherschutz und Lebensmittelsicherheit).

Tissue Preparation and Immunocytochemistry

The animals were anesthetized with an overdose of ketamin (Essex Tierarznei) and transcardially perfused with 0.9% NaCl solution to remove blood from vessels, followed by 4% paraformaldehyde dissolved in 0.1 M phosphate buffer (PB, pH 7.4). The brains were removed and the two hemispheres separated. The left hemispheres were flattened (Welker and Woolsey, 1974) whereas the right ones were kept unmodified, and all tissue was postfixed for 2 h in the same fixative. The right hemispheres were cut in the coronal plane, the left hemispheres tangentially on a vibratome (VT 1200S, Leica), both with a nominal section thickness of 50 μm.

The sections of PV-GIN animals were incubated with rabbit anti-GFP (Invitrogen) 1:2500 in TRIS-buffered saline with 0.3% Triton X-100 (TBST) for 2 days (in a cold room), followed by an anti-rabbit IgG coupled with Alexa-488 (Invitrogen) 1:500 in TBST for 2 h. The PV+ cells contained a sufficient amount of tdTomato, therefore they did not need further signal amplification. The sections of SSTcre/tdTomato and VIPcre/tdTomato animals were stained with guinea pig anti-vesicular glutamate transporter 2 (vGlut2; Millipore) 1:10,000 in TBST for 2 days, followed by an anti-guinea pig IgG coupled with Alexa 488 (Invitrogen) 1:500 in TBST for 2 h, in order to identify barrels. In a last step, sections of all strains were stained with DAPI (1:1000, Molecular Probes) to label cell nuclei. The sections were then embedded in AquaPolymount (Polysciences).

Image Acquisition

Microphotographs were taken with an epifluorescence microscope (AxioImager.M2, Zeiss, Jena, Germany; 5x A-Plan objective, NA 0.12 or 10x C-Plan Neofluar objective, NA 0.3) as "virtual tissue photomontages" controlled by Neurolucida software (MBF Bioscience, Colchester, VT, United States). Filter sets used were: for DAPI #49 (BP 365; BS 395, BP 445/50), for Alexa488/GFP #44 (BP 475/40; BS 500, BP 530/50), and for tdTomato #45 (Bp 560/40; BS 585, BP 630/75. To maintain illumination intensity comparable across sections, the dynamic range was set according to the saturation of a few (3–5) brightest pixels that belonged to somata.

Data Extraction

Please consult **Supplementary Figure 1** for a more intuitive illustration of the work flow. Consecutive tangential sections were aligned according to the pattern of vertically oriented cortical blood vessels. Neurolucida was used for registering cells and cortical domains. First, the barrels were identified and labeled individually, based on DAPI staining that was correlated with either intense PV neuropil or vGluT2 immunostaining, which is caused by thalamocortical projections into layer (L) IV. In coronal sections, the borders between LI, LII/LIII and LVa, LVb, and LVI were identified on the basis of DAPI staining. The pia mater and the LVI/white matter border were also delineated throughout the entire barrel field. Then, the location of all PV, SST, and VIP cells was registered independent of the laminar boundaries, thus the borders of the cortical domains did not bias the data collection. The resulting data files were analyzed in Neurolucida Explorer (MBF Biosciences). The following parameters were extracted: (i) cell numbers, (ii) areas of all delineated cortical domains (barrels, septa, and the related layers of the respective cortical columns), and (iii) the coordinates of all the GABAergic neurons with their distance from pia mater and white matter.

Data Processing

After identifying each barrel in coronal sections, the depth of the borders between cortical layers was measured for each, and the medio-lateral and rostro-caudal coordinates were also registered. These parameters were used to correct the measured volumina of the flattened tangential sections. After that procedure, the tangential sections were re-binned into 20 sections. In coronal sections we found the cortical thickness to be 1019,164 ± 38,550 μm. In case of 50 μm-thick sections it would contain a total number of ca. 20 tangential sections. By cutting the brain tangentially, we had diverse section numbers (15–19), depending on applied pressure during flattening. Therefore, we standardized the cortical thickness through re-binning the

sections with the following methods. First we divided each section in 20 virtual subsections and divided the cell count of a given section equally between its virtual subsections. For example, in an animal with $n = 17$ sections ($n =$ original section number), we got $n' = 340$ subsections ($n' =$ number of a new subsection, $n' = n^* 20$). Then, we created normalized tangential sections: one 20th of n' of all subsections were binned together (in the example above, 17 subsections were binned in one new normalized section (**Supplementary Figure 2**).

The densities of cells of interest (PV+, SST+, VIP+) were plotted and the borders of cortical layers were defined, using the inflection points of these curves (Pohlkamp et al., 2014). Since the cortical and laminar thickness varies according to rostro-caudal and medio-lateral position, the extracted raw data had to be transformed to obtain statistically comparable quantities. The normalization of cortical thickness utilized landmarks, e.g., points of inflection on laminar borders as described previously for each of the markers examined (Pohlkamp et al., 2014). This normalization process transformed all the data into the same thickness range, therefore it made the comparison (or pooling) of coronally- versus tangentially-cut as well as more rostrally or medially versus more caudally or laterally located tissue possible.

To determine whether our data showed Gaussian distribution, we used the Shapiro–Wilk normality test. Since the Shapiro–Wilk test failed in all cases of studied cell types, the non-parametric Kruskal–Wallis test was used to determine statistically significant differences. Alpha levels were adjusted with the Bonferroni method. For comparison of numbers from tangential versus coronal sections, data were plotted and the correlation coefficient was calculated (Mystat, Systat Software, Inc., United States). We collected data from coronal sections to compare our results to previous literature. Tangential section were used to collect data about absolute numbers in the whole posteromedial barrelfield and because the identification of barrels and interbarrel septa was much more obvious. Coronal and tangential data series correlated highly with each other, therefore the density values of coronal and tangential section were pooled for the analysis.

RESULTS

PVcre/tdTomato-Expressing (PV+) GABAergic Neurons

These cells show a dominant location within the termination zones of the lemniscal thalamic projections (Chmielowska et al., 1989; Wimmer et al., 2010b), namely LIV and the LVb/VI border but also within the termination zone of paralemniscal thalamic projections (Wimmer et al., 2010b), namely layer Va (**Figure 1A**). Indeed, 26.17 ± 2.73% of all PV+ cells were located in LIV, 14.84 ± 1.94% in LVa and 27.15 ± 1.49% in LVb, whereas in layers II/III and VI together only 31.83 ± 1.99% were found. In LIV, the neuropil labeling led to the clear delineation of barrels, in coronal as well as tangential sections (**Figures 1A,B**).

Laminar Distribution

We studied the PV+ cell distribution in coronal sections of 3 hemispheres and in tangential sections of another 3 hemispheres. The coronal and tangential sections correlated with each other in terms of cell number and distribution ($n = 6$; $r^2 = 0.925$) (**Figure 3D**), therefore they were pooled for further analysis (**Table 1** and **Figure 3A**).

When extrapolated in number to 1 mm^3, PV+ cells preferred LIV and LV (a and b) in approximately equal numbers, were much sparser in LII/III and LVI and avoided LI (**Table 1** and **Figures 1A,B**, **3**; significance levels are listed in **Supplementary Table 1**, Kruskal–Wallis test was used to determine statistically significant differences). Thus, PV+ cell numbers showed a differential distribution between layers, which was very similar in the two analyzed columnar compartments (see also below).

Columnar (Barrel Versus Septum) Distribution

In layers II throughout VI, the distribution of PV+ cells was found to be similar for barrel- and septum-related compartments. However, this more or less even distribution of cell bodies was masked by the differential distribution of PV+ neuropil, which strongly preferred barrels (**Figure 1B** and **Table 1**). There were slightly more cells in barrels versus septa (**Figures 2A,D,G,J**, **3A**, LIVc versus LIVs), but this difference was not statistically significant ($p = 0.885$; significance levels are listed in **Supplementary Table 2**, Kruskal–Wallis test was used to determine statistically significant differences). Considering soma and neuropil labeling in PV+ neurons, in LIV this resulted in a complementary distribution profile, contrasting with VIP+ and SST+ GABAergic neurons (see below).

SST-Expressing (SST+) GABAergic Neurons

The overall distribution of SST+ cells was unique in several aspects (**Figures 1C,D**). Whereas PV+ cells showed an increased density in layers IV and Vb (as noted above), SST+ cells strongly preferred infragranular layers V-VI. In fact, 73.69 ± 5.37% of the cells were located in the infragranular layers, whereas only 26.31 ± 5.37% were found in layers I-IV. This suggests that projections like the one from M1 with heavy terminal labeling in infragranular layers might be a preferential input to these neurons (Kinnischtzke et al., 2014) but also that paralemniscal inputs have ample opportunity in targeting this class of cells in LI and LVa, whereas lemniscal inputs should preferentially innervate cells in LVb/LVI (Wimmer et al., 2010b; Audette et al., 2017).

Laminar Distribution

We studied the SST+ cell distribution in coronal sections of 3 hemispheres and in tangential sections of another three hemispheres, too. The coronal and tangential sections (total $n = 6$) correlated highly with each other ($r^2 = 0.94$) (**Figure 3D**), therefore the neurons were pooled for further analysis (**Table 2** and **Figure 3B**).

The SST+ neurons were similar in number in layers Va, Vb, and VI. Each of these layers possessed significantly more cells than LIV, LII/III, and LI, respectively. LII/III SST+ cells did not differ in number from LIV cells. The lowest number of SST+ cells was found in LI, which was significantly different from

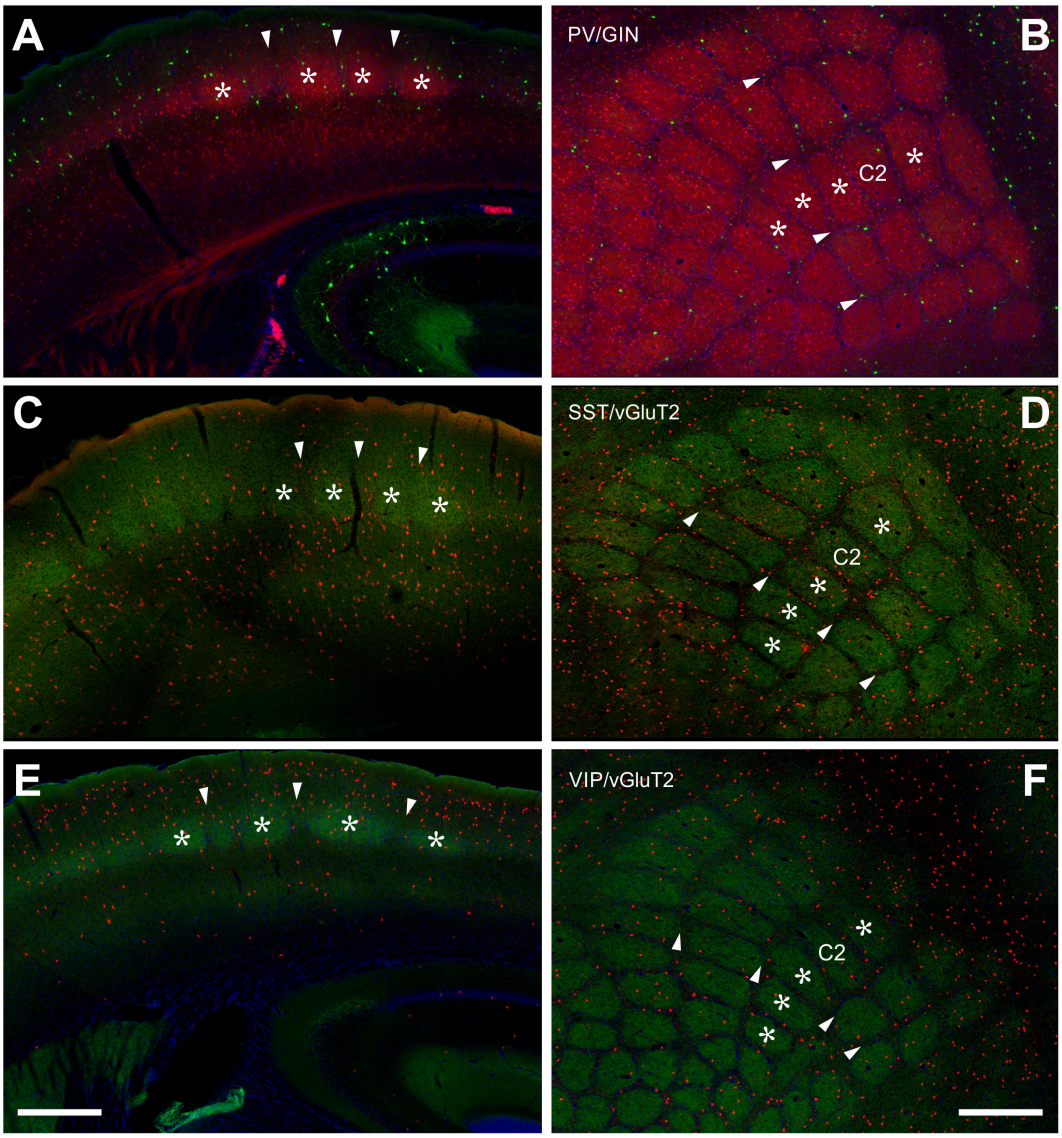

FIGURE 1 | Localization of PV+, SST+, and VIP+ interneurons in the barrel cortex. **(A,B)** Double labeling of PV+ (red, from PVcre/tdTomato animals) and SST+ (green, GIN line) shows a clear delineation of barrel-related columns in the coronal section **(A)** and a whisker-related somatotopic pattern in layer IV of tangential sections **(B)**. Indication of barrels (*asterisks*) and septa (*arrowheads*) holds for all images. PV+ cells seem to prefer barrels, but quantitative analysis showed that the cell bodies are distributed homogenously. GIN cells, however, displayed an obvious preference for the septal compartment. **(C,D)** SST+ cells (red, from SSTcre/tdTomato animals) were located preferentially in the infragranular layers **(D)**, somewhat aligned to interbarrel septa **(C,D)**. VGluT2 (green) strongly labels the lemniscal thalamic termination zone in layer IV barrels. **(E,F)** VIP+ cells (red; from VIPcre/tdTomato animals) preferred supragranular layers **(E)** and interbarrel septa **(F)**. Scale bars: 500 μm.

all other layers (significance levels are listed in **Supplementary Table 3**; Kruskal–Wallis test was used to determine statistically significant differences).

Columnar (Barrel Versus Septum) Distributions

When comparing the barrel with the septal compartment, we found that SST+ cells were distributed more or less homogenously between these compartments in all layers, except LIV (**Table 2**). As shown in **Figures 2B,E,H,K**, **3B**, in LIV, the septal compartment contained significantly more cells than the barrel compartment ($p < 0.0001$) (significance levels are listed in **Supplementary Table 4**; Kruskal–Wallis test was used to determine statistically significant differences).

VIP-Expressing (VIP+) GABAergic Neurons

Interestingly, VIP+ cells show an inverse relationship to SST+ cells, as they display a strong preference for the supragranular layers (**Figure 1E**). Indeed, 70.24% of all cells were located

TABLE 1 | Cell density of PV-expressing neurons, differentiated by barrel column and septum.

	Cell density in column (1/mm^3)	± SD (1/mm^3)	Cell density in septum (1/mm^3)	± SD (1/mm^3)
Layer I	0	0	0	0
Layer II/III	4995.65	1278.58	5050.46	2012.55
Layer IV	8426.59	1405.35	8252.19	1751.12
Layer Va	8510.96	1766.67	7904.56	2217.68
Layer Vb	8964.038	2143.11	8244.73	3170.58
Layer VI	3017.66	1003.13	2766.40	877.38

in layers I-III, whereas only 29.76% were found in layers IV-VI. Since the subpopulation located in LI and LII/III shows extensive dendritic arborization in layer I (Prönneke et al., 2015), projections like those from motor cortex or basal forebrain can strongly target these cells (Mechawar et al., 2000; Lee et al., 2013), as does the lemniscal thalamus in deep LII/III (Staiger et al., 1996b; Wall et al., 2016).

Laminar Distribution

We studied the VIP+ cell distribution in coronal sections of three hemispheres and in tangential sections of another three hemispheres. The cell numbers in these sections (total $n = 6$) were again correlated highly with each other ($r^2 = 0.973$) (**Figure 3D**), thus, the values were pooled for further analysis (**Table 3** and **Figure 3C**).

VIP+ cells in LII/III outnumbered those in all other layers significantly whereas LI had significantly lower numbers than all other layers (except LVI). Also the gradient from LIV to LVI reached statistical significance, with each deeper layer housing less neurons than the one located pialward (significance levels are listed in **Supplementary Table 5**; Kruskal–Wallis test was used to determine statistically significant differences).

Columnar (Barrel Versus Septum) Distribution

When comparing the columnar and septal compartments, there was no obvious difference in the supragranular and infragranular layers. However, in LIV we found significantly more cells in septa than in barrels ($p < 0.0001$; Kruskal–Wallis test was used to determine statistically significant differences), which can be seen in **Figures 1F**, **2C,F,I,L**, **3C**. This columnar segregation was therefore restricted to the granular layer where the cell density in septa was approximately two times higher than in barrels (significance levels are listed in **Supplementary Table 6**; Kruskal–Wallis test was used to determine statistically significant differences).

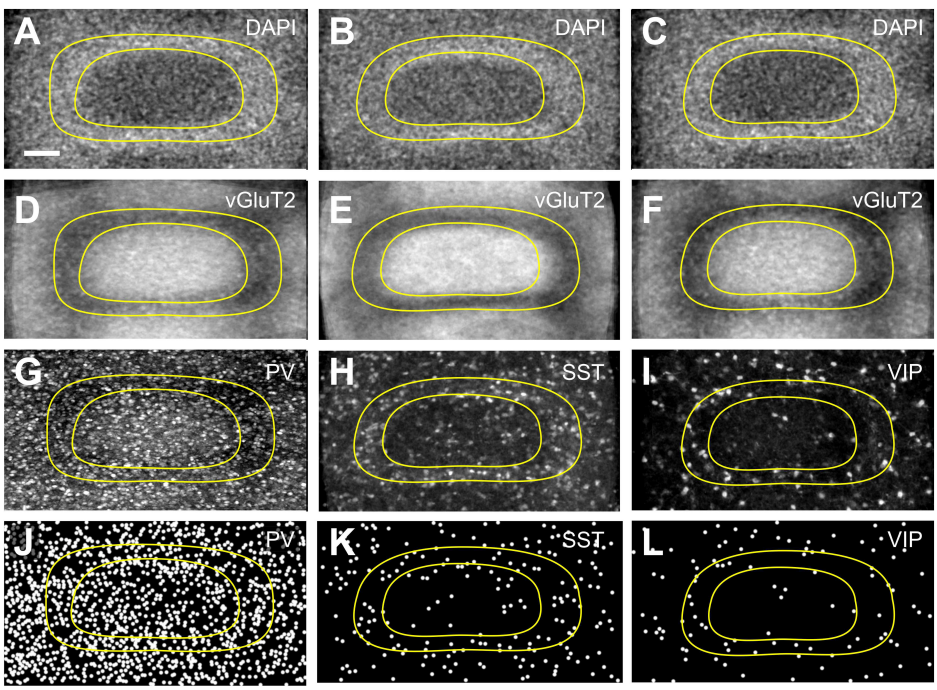

FIGURE 2 | Distribution of interneurons across layer IV barrels and septa. Fine-grained distribution of **(A,D,G,J)** PV+, **(B,E,H,K)** SST+, and **(C,F,I,L)** VIP+ interneuron somata, using tangential sections to allow a better delineation of septal and barrel compartments. DAPI staining **(A–C)** or vGluT2 immunostaining **(D–F)** was used to reveal the border of the barrels in a complementary manner. Images of nominally 50 μm thick sections of PV+ **(G)**, SST+ **(H),** and VIP+ **(I)** somata and neuropil, in conjunction with the respective Neurolucida reconstructions **(J–L)** reveal a homogenous distribution of PV+ as well as a septal preference of SST+ and VIP+ cells. Since SST and VIP neurons appear in a quite low density, especially in the granular layer, we had to project numerous barrels onto each other, in order to be able to display the uneven distribution of these cells. For that purpose, we collected barrels, which could be fit into an idealized (averaged) barrel, and then the images were projected to a single image plane using ImageJ Sum Slices function. This was not necessary for PV cells since the cell density was much higher, but for the sake of comparability we performed the same protocol on PV images. Scale bars: 50 μm.

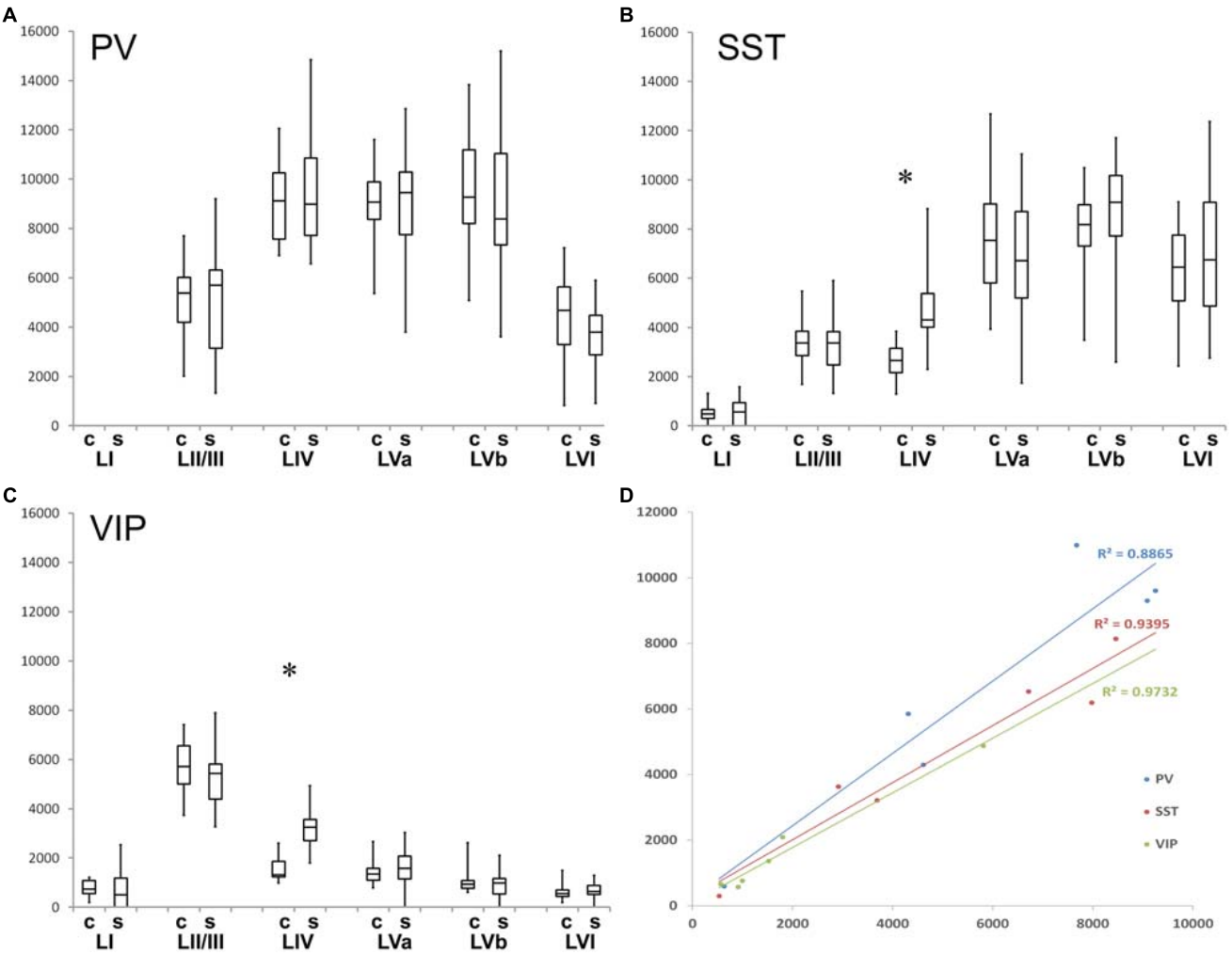

FIGURE 3 | Quantification of layer- and column-related distribution of GABAergic interneurons. Box and whisker plot of laminar density of **(A)** PV+, **(B)** SST+, and **(C)** VIP interneurons. Note the statistically significant difference between barrel column (C)- and septum (S)-associated compartments for VIP+ and SST+ cells in layer IV. Significant laminar distribution differences were not denoted because of figure transparency, details were explained above. The graphs also show that all of the studied interneurons completely (PV+) or largely (SST+, VIP+) avoid LI. **(D)** Diagram shows the cell densities of coronal versus tangential sections. Correlation coefficients (R) are close to 1, so the numbers are highly correlated to each other ($R_{PV.}$ = 0.925; R_{SST} = 0.940; R_{VIP} = 0.973).

In summary, we could reproduce the general pattern of a dominance of PV+ cells in lemniscal thalamorecipient layers (LIV and Vb) but show a frequent occurrence on the paralemniscal thalamorecipient LVa, too. SST+ showed a strong abundance in LVa/b and LVI whereas VIP+ were preferentially distributed in LII/III and LIV (**Supplementary Figure 3**). In addition, when comparing barrel-related columns with septum-associated compartments, only in LIV we could detect a statistically significant preference of SST+ and VIP+ cells for the latter (**Supplementary Figure 3**).

DISCUSSION

In the present study, we confirmed and extended the laminar distribution profiles of major subpopulations of GABAergic neurons in the mouse barrel cortex (for recent reviews see Staiger et al., 2015; Tremblay et al., 2016; Feldmeyer et al., 2018). In agreement with these previous studies, we show in tdTomato-expressing mouse lines that PV+ cells prefer layers IV and Vb, whereas SST+ cells prefer all infragranular and VIP+ cells supragranular (LII/III) layers. We extend these findings by showing that PV+ cells do not have a preferential localization within columnar compartments, since cell counts show a very similar distribution between barrel column- and septum-associated compartments. Thus, it is an anisotropic distribution of PV+ neuropil labeling that accentuates barrels in coronal as well as tangential sections. On the other hand, SST+ and VIP+ cells were significantly more frequent in the septum than the barrel (in LIV), whereas this unique distribution was just a trend, if anything, outside of LIV. These findings led us to propose that different subpopulations of neocortical GABAergic

TABLE 2 | Cell density of SST-expressing neurons, differentiated by barrel column and septum.

	Cell density in column (1/mm^3)	± SD (1/mm^3)	Cell density in septum (1/mm^3)	± SD (1/mm^3)
Layer I	512.67	356.23	566.29	558.33
Layer II/III	3353.63	903.46	3318.67	1159.57
Layer IV	2661.42	697.03	4772.67	1535.58
Layer Va	7594.97	2459.81	6752.20	2268.18
Layer Vb	8064.99	1587.00	8675.49	2425.20
Layer VI	6344.08	1985.93	6856.99	2454.67

TABLE 3 | Cell density of VIP-expressing neurons, differentiated by barrel column and septum.

	Cell density in column (1/mm^3)	± SD (1/mm^3)	Cell density in septum (1/mm^3)	±SD (1/mm^3)
Layer I	788.87	335.88	571.67	536.68
Layer II/III	5596.69	968.70	5150.93	1090.85
Layer IV	1574.74	481.32	3204.72	908.99
Layer Va	1448.33	492.38	1594.11	709.10
Layer Vb	1007.70	454.04	852.38	596.40
Layer VI	630.11	285.53	672.18	313.03

neurons could be differentially associated with different input pathways, as initially suggested for the archicortex (Somogyi et al., 1998). This notion was also referred to in the sensorimotor cortex (Kubota et al., 2007; Cruikshank et al., 2010; Audette et al., 2017), although these, as well as more recent studies in auditory and visual cortex, did not reveal a very refined picture (Ji et al., 2016). Since it is obvious that soma location is only a poor predictor for the entire input space of a neuron, we and others are currently trying to substantiate the hypothesis of thalamic (and other) input specificity on different classes of GABAergic neurons with optogenetics and whole cell recordings.

Technical Considerations

We compared and finally pooled results obtained from coronal and tangential sections of the barrel cortex (Woolsey and van der Loos, 1970). The advantage of frontal sectioning is that laminar borders can be identified with high certainty, whereas in tangential sections the barrel versus septal regions can be delineated unequivocally. Since tangential sectioning requires a certain compression of the cortex, and the cortex is not evenly thick along its medio-lateral axis, the distance of the cells from the pia mater had to be adjusted, in order to match laminar location in tangential with coronal sections. After adjustment, the cell density read-out from coronal and tangential sections was virtually identical, allowing us to pool the data. Our laminar density results of VIP+ cells are in very good agreement with that previously described for the barrel cortex (Prönneke et al., 2015) and with PV+ and SST+ cell counts from other ongoing projects (own unpublished results).

Here, we used staining for vGlut2 and DAPI as pre- and postsynaptic markers, respectively, to determine barrel and septum borders, building on our previous experience (Wagener et al., 2010). Because of putative plasticity of thalamocortical fibers (Wimmer et al., 2010a), the vGlut2-defined barrel borders could vary, thus the additional use of DAPI staining is important to define the actual barrel size and further helps to distinguish barrel and septal compartments (Erzurumlu and Kind, 2001).

It should also be noted that we have counted tdTomato-expressing cell bodies distributed across the various layers and columns, which does not necessarily mean that they are specifically and comprehensively reflecting the entire population of interest, as represented by the different cre-driver lines. However, previous studies already showed a reasonable overlap of tdTomato-fluorescence with the respective markers (GAD1, PV, SST, and VIP (Taniguchi et al., 2011; Pfeffer et al., 2013); and our own published and still ongoing efforts to characterize these mouse lines revealed a very high specificity and an excellent sensitivity (Prönneke et al., 2015).

Comparison to Previous Studies

To the best of our knowledge, the numbers of GABAergic neurons in mouse barrel cortex had not been established before and the partitioning of GABAergic neurons between barrel- and septal column was completely lacking. It has to be acknowledged that there is a comprehensive quantification with an immunohistochemical approach available, the area-densities reported there being in general agreement with our results (Xu et al., 2010). Here, we started to overcome this lack of detailed knowledge by counting soma numbers of neurons expressing tdTomato-fluorescence under the control of three marker genes that are currently viewed as the best candidates to separate the population of GABAergic neurons into three different classes (Taniguchi et al., 2011; Tremblay et al., 2016).

In PVcre/tdTomato mice, we could detect a distribution across layers that was both, qualitatively and quantitatively similar to the rat somatosensory cortex (van Brederode et al., 1991; Ren et al., 1992). We showed numbers peaking in layers IV, Va, and Vb, which would mean that major layers receiving lemniscal or paralemniscal input (Wimmer et al., 2010b) house a feedforward inhibition motif in their circuitry (Cruikshank et al., 2010; Naka and Adesnik, 2016), which does strongly influence their *in vivo* physiology (Bruno and Sakmann, 2006; de Kock et al., 2007; Yu et al., 2016).

Surprisingly, in tangential sections we did not find a significant difference between barrel and septal compartments, although PV has been used as a marker for barrels (Sukhov et al., 2016). This means that barrels are highlighted in PV staining by virtue of the neuropil labeling (mainly being axonal boutons) and not by somatodendritic profiles. This could be explained by anisotropic axonal arbors of basket cells displaying a bias toward barrel centers (Munoz et al., 2014; Koelbl et al., 2015). Further evidence that there is a profound difference between the organization of PV+ cells' dendrites versus axons in barrels versus septa comes from a recent study that showed their gap junction coupling to occur in a cell type- and location-specific manner (Shigematsu et al., 2018).

In SSTcre/tdTomato mice, we were able to show that all infragranular layers express high numbers of these cells, where

they recently have been shown also to be most diverse in structure and function (Nigro et al., 2018). In contrast, the fewer cells located in LII/III all seem to be Martinotti cells (Munoz et al., 2017; Nigro et al., 2018), which was also consistently reported in the GIN mouse line (Oliva et al., 2000; Ma et al., 2006; Walker et al., 2016). The minority population in LI remains to be better characterized (Ma et al., 2014).

The analysis in tangential sections, revealing a preferential location in septa when compared to barrels, is without precedent. One has to know that septa in mice are very small compartments, as compared to rats, thus it is very difficult to specifically record from them, in order to assess their function (Welker and Woolsey, 1974). We can only speculate that the increased number of SST+ neurons (but also VIP+ cells, see below) might serve to flexibly adjust the receptive field size of septal neurons, which is usually larger than that of barrel-related column neurons (Brecht and Sakmann, 2002).

In VIPcre/tdTomato mice, we obtained cell numbers across the different layers that were in good agreement with previous reports (Xu et al., 2010; Prönneke et al., 2015), pinpointing a preferential role of these neurons to relay information originating from diverse sources via axonal projections into layers I-III. This information is then relayed to all layers of the respective barrel column- or septum-associated compartment by virtue of their "column-filling" axonal arbors, probably impinging on excitatory and inhibitory neurons in parallel (Garcia-Junco-Clemente et al., 2017; Kuchibhotla et al., 2017; Zhou et al., 2017).

As noted already above, a novel finding was the differential distribution of VIP+ somata in barrels versus septa, with approximately twice as many cells in the septa than in the barrels. Interestingly, a previous study has reported a differential distribution of VIP+ boutons, which were more numerous in the side region than within the hollow (Zilles et al., 1993). Since a "side" is the barrel wall and the septum pooled (Welker and Woolsey, 1974) and since VIP neurons in layer II/III and IV have a radially restricted axonal arbor (Prönneke et al., 2015), these findings are complementary to ours.

Functional Implications

As noted above, the soma location alone is a very limited predictor of the input space of a neuron. However, since the dendritic arbors of GABAergic neurons are usually more compact than those of pyramidal cells, this could serve as a reasonable first approximation to consider the layer- and column-associated location of the soma as the main input space of the respective neuron (De Felipe et al., 2013).

Thus, we suggest that PV+ neurons are more or less uniformly distributed to fulfill the need of all cortical circuits to operate in a tight excitation-inhibition-balance (Isaacson and Scanziani, 2011), no matter whether feedforward pathways from the thalamus or local pathways activate them. SST+ cells, with their strong bias to infragranular layers and to LIV septa, are rather heterogeneous in their input and output domains, making a more specific functional interpretation than that they are providing widespread dendritic inhibition difficult (Urban-Ciecko and Barth, 2016; Yavorska and Wehr, 2016). VIP+ neurons, with their strong bias to supragranular layers and also LIV septa, can directly participate in sensory processing, potentially by strong disinhibitory mechanisms (Karnani et al., 2016a,b; Walker et al., 2016; Feldmeyer et al., 2018) but they also relay more global salience- or reward-related signals, originating in (pre-)motor cortex or in subcortical neuromodulatory centers to the column (Lee et al., 2013; Kepecs and Fishell, 2014).

The enrichment of SST+ and VIP+ neurons in LIV LIV septa might help to task-dependently switch cortical activity flow (and thus sensory processing) between the nested, partly distinct, partly overlapping, circuits that originate in or are wired through barrel- versus septum-associated compartments of the barrel cortex (Alloway, 2008; Diamond et al., 2008; Feldmeyer et al., 2013). The next task will be to perform optogenetic stimulation of these putative input pathways and record from single identified GABAergic neurons, in order to test our predictions.

AUTHOR CONTRIBUTIONS

ZA and CD conceived and performed the experiments, analyzed the results, and co-wrote the manuscript. MW provided the materials and co-wrote the manuscript. JS conceived the experiments, supervised the project, and wrote the manuscript.

FUNDING

This work was supported by the Deutsche Forschungsgemeinschaft (DFG grant STA 431/14-1).

ACKNOWLEDGMENTS

We want to thank Dr. Robin Wagener for his help with getting the project started. We are grateful to Patricia Sprysch for excellent technical assistance.

SUPPLEMENTARY MATERIAL

The Supplementary Material for this article can be found online at: https://www.frontiersin.org/articles/10.3389/fnana.2019.00045/full#supplementary-material

REFERENCES

Alloway, K. D. (2008). Information processing streams in rodent barrel cortex: the differential functions of barrel and septal circuits. *Cereb. Cortex* 18, 979–989. doi: 10.1093/cercor/bhm138

Alloway, K. D., Zhang, M. L., and Chakrabarti, S. (2004). Septal columns in rodent barrel cortex: Functional circuits for modulating whisking behavior. *J. Comp. Neurol.* 480, 299–309. doi: 10.1002/cne.20339

Audette, N. J., Urban-Ciecko, J., Matsushita, M., and Barth, A. L. (2017). POm thalamocortical input drives layer-specific microcircuits in

somatosensory cortex. *Cereb. Cortex* 28, 1312–1328. doi: 10.1093/cercor/bhx044

Bayraktar, T., Welker, E., Freund, T. F., Zilles, K., and Staiger, J. F. (2000). Neurons immunoreactive for vasoactive intestinal polypeptide in the rat primary somatosensory cortex: morphology and spatial relationship to barrel-related columns. *J. Comp. Neurol.* 420, 291–304. doi: 10.1002/(SICI)1096-9861(20000508)420:3<291::AID-CNE2>3.0.CO;2-H

Brecht, M., and Sakmann, B. (2002). Dynamic representation of whisker deflection by synaptic potentials in spiny stellate and pyramidal cells in the barrels and septa of layer 4 rat somatosensory cortex. *J. Physiol. (Lond.)* 543, 49–70. doi: 10.1113/jphysiol.2002.018465

Bruno, R. M., and Sakmann, B. (2006). Cortex is driven by weak but synchronously active thalamocortical synapses. *Science* 312, 1622–1627. doi: 10.1126/science.1124593

Bureau, I., Saint Paul, F., and Svoboda, K. (2006). Interdigitated paralemniscal and lemniscal pathways in the mouse barrel cortex. *PLoS Biol.* 4:e382. doi: 10.1371/journal.pbio.0040382

Caputi, A., Rozov, A., Blatow, M., and Monyer, H. (2009). Two calretinin-positive GABAergic cell types in layer 2/3 of the mouse neocortex provide different forms of inhibition. *Cereb. Cortex* 19, 1345–1359. doi: 10.1093/cercor/bhn175

Celio, M. R. (1986). Parvalbumin in most gamma-aminobutyric acid-containing neurons of the rat cerebral cortex. *Science* 231, 995–997. doi: 10.1126/science.3945815

Chmielowska, J., Carvell, G. E., and Simons, D. J. (1989). Spatial organization of thalamocortical and corticothalamic projection systems in the rat SmI barrel cortex. *J. Comp. Neurol.* 285, 325–338. doi: 10.1002/cne.902850304

Cruikshank, S. J., Urabe, H., Nurmikko, A. V., and Connors, B. W. (2010). Pathway-specific feedforward circuits between thalamus and neocortex revealed by selective optical stimulation of axons. *Neuron* 65, 230–245. doi: 10.1016/j.neuron.2009.12.025

David, C., Schleicher, A., Zuschratter, W., and Staiger, J. F. (2007). The innervation of parvalbumin-containing interneurons by VIP-immunopositive interneurons in the primary somatosensory cortex of the adult rat. *Eur. J. Neurosci.* 25, 2329–2340. doi: 10.1111/j.1460-9568.2007.05496.x

De Felipe J., López-Cruz P. L., Benavides-Piccione, R., Bielza, C., Larrañaga, P., et al. (2013). New insights into the classification and nomenclature of cortical GABAergic interneurons. *Nat. Rev. Neurosci.* 14, 202–216. doi: 10.1038/nrn3444

de Kock, C. P. J., Bruno, R. M., Spors, H., and Sakmann, B. (2007). Layer and cell type specific suprathreshold stimulus representation in primary somatosensory cortex. *J. Physiol. (Lond.)* 581, 139–154. doi: 10.1113/jphysiol.2006.124321

Diamond, M. E., Von Heimendahl, M., Knutsen, P. M., Kleinfeld, D., and Ahissar, E. (2008). 'Where' and 'what' in the whisker sensorimotor system. *Nat. Rev. Neurosci.* 9, 601–612. doi: 10.1038/nrn2411

Erzurumlu, R. S., and Kind, P. C. (2001). Neural activity: sculptor of 'barrels' in the neocortex. *Trends Neurosci.* 24, 589–595. doi: 10.1016/S0166-2236(00)01958-5

Feldmeyer, D., Brecht, M., Helmchen, F., Petersen, C. C. H., Poulet, J. F. A., Staiger, J. F., et al. (2013). Barrel cortex function. *Prog. Neurobiol.* 103, 3–27. doi: 10.1016/j.pneurobio.2012.11.002

Feldmeyer, D., Qi, G., Emmenegger, V., and Staiger, J. F. (2018). Inhibitory interneurons and their circuit motifs in the many layers of the barrel cortex. *Neuroscience* 368, 132–151. doi: 10.1016/j.neuroscience.2017.05.027

Garcia-Junco-Clemente, P., Ikrar, T., Tring, E., Xu, X., Ringach, D. L., and Trachtenberg, J. T. (2017). An inhibitory pull-push circuit in frontal cortex. *Nat. Neurosci.* 20, 389–392. doi: 10.1038/nn.4483

Hajós, F., Zilles, K., Zsarnovszky, A., Sotonyi, P., Gallatz, K., and Schleicher, A. (1998). Modular distribution of vasoactive intestinal polypeptide in the rat barrel cortex: changes induced by neonatal removal of vibrissae. *Neuroscience* 85, 45–52. doi: 10.1016/S0306-4522(97)00590-3

Harris, K. D., and Mrsic-Flogel, T. D. (2013). Cortical connectivity and sensory coding. *Nature* 503, 51–58. doi: 10.1038/nature12654

Harris, K. D., and Shepherd, G. M. G. (2015). The neocortical circuit: themes and variations. *Nat. Neurosci.* 18, 170–181. doi: 10.1038/nn.3917

Huang, Z. J. (2014). Toward a genetic dissection of cortical circuits in the mouse. *Neuron* 83, 1284–1302. doi: 10.1016/j.neuron.2014.08.041

Isaacson, J. S., and Scanziani, M. (2011). How inhibition shapes cortical activity. *Neuron* 72, 231–243. doi: 10.1016/j.neuron.2011.09.027

Ji, X. Y., Zingg, B., Mesik, L., Xiao, Z. J., Zhang, L. I., and Tao, H. Z. W. (2016). Thalamocortical innervation pattern in mouse auditory and visual cortex: laminar and cell-type specificity. *Cereb. Cortex* 26, 2612–2625. doi: 10.1093/cercor/bhv099

Jiang, X. L., Shen, S., Cadwell, C. R., Berens, P., Sinz, F., Ecker, A.S., et al. (2015). Principles of connectivity among morphologically defined cell types in adult neocortex. *Science* 350:aac9462. doi: 10.1126/science.aac9462

Karnani, M. M., Jackson, J., Ayzenshtat, I., Sichani, A. H., Manoocheri, K., Kim, S., et al. (2016a). Opening holes in the blanket of inhibition: localized lateral disinhibition by VIP interneurons. *J. Neurosci.* 36, 3471–3480. doi: 10.1523/JNEUROSCI.3646-15.2016

Karnani, M. M., Jackson, J., Ayzenshtat, I., Tucciarone, J., Manoocheri, K., Snider, W. G., et al. (2016b). Cooperative subnetworks of molecularly similar interneurons in mouse neocortex. *Neuron* 90, 86–100. doi: 10.1016/j.neuron.2016.02.037

Kepecs, A., and Fishell, G. (2014). Interneuron cell types are fit to function. *Nature* 505, 318–326. doi: 10.1038/nature12983

Kim, U., and Ebner, F. F. (1999). Barrels and septa: separate circuits in rat barrel field cortex. *J. Comp. Neurol.* 408, 489–505. doi: 10.1002/(SICI)1096-9861(19990614)408:4<489::AID-CNE4>3.0.CO;2-E

Kinnischtzke, A. K., Simons, D. J., and Fanselow, E. E. (2014). Motor cortex broadly engages excitatory and inhibitory neurons in somatosensory barrel cortex. *Cereb. Cortex* 24, 2237–2248. doi: 10.1093/cercor/bht085

Koelbl, C., Helmstaedter, M., Lubke, J., and Feldmeyer, D. (2015). A barrel-related interneuron in layer 4 of rat somatosensory cortex with a high intrabarrel connectivity. *Cereb. Cortex* 25, 713–725. doi: 10.1093/cercor/bht263

Kubota, Y., Hatada, S., Kondo, S., Karube, F., and Kawaguchi, Y. (2007). Neocortical inhibitory terminals innervate dendritic spines targeted by thalamocortical afferents. *J. Neurosci.* 27, 1139–1150. doi: 10.1523/JNEUROSCI.3846-06.2007

Kubota, Y., Kondo, S., Nomura, M., Hatada, S., Yamaguchi, N., Mohamed, A. A., et al. (2015). Functional effects of distinct innervation styles of pyramidal cells by fast spiking cortical interneurons. *Elife* 4, 1–27. doi: 10.7554/eLife.07919

Kuchibhotla, K. V., Gill, J. V., Lindsay, G. W., Papadoyannis, E. S., Field, R. E., Sten, T. A. H., et al. (2017). Parallel processing by cortical inhibition enables context-dependent behavior. *Nat. Neurosci.* 20, 62–71. doi: 10.1038/nn.4436

Lee, S., Kruglikov, I., Huang, Z. J., Fishell, G., and Rudy, B. (2013). A disinhibitory circuit mediates motor integration in the somatosensory cortex. *Nat. Neurosci.* 16, 1662–1670. doi: 10.1038/nn.3544

Lu, S. M., and Lin, R. C. S. (1993). Thalamic afferents of the rat barrel cortex: a light- and electron-microscopic study using *Phaseolus vulgaris* leucoagglutinin as an anterograde tracer. *Somatosens Motor Res.* 10, 1–16. doi: 10.3109/08990229309028819

Ma, J., Yao, X. H., Fu, Y. H., and Yu, Y. C. (2014). Development of layer 1 neurons in the mouse neocortex. *Cereb. Cortex* 24, 2604–2618. doi: 10.1093/cercor/bht114

Ma, Y. Y., Hu, H., Berrebi, A. S., Mathers, P. H., and Agmon, A. (2006). Distinct subtypes of somatostatin-containing neocortical interneurons revealed in transgenic mice. *J. Neurosci.* 26, 5069–5082. doi: 10.1523/JNEUROSCI.0661-06.2006

Maffei, A. (2017). Fifty shades of inhibition. *Curr. Opin. Neurobiol.* 43, 43–47. doi: 10.1016/j.conb.2016.12.003

Markram, H., Toledo-Rodriguez, M., Wang, Y., Gupta, A., Silberberg, G., and Wu, C. Z. (2004). Interneurons of the neocortical inhibitory system. *Nat. Rev. Neurosci.* 5, 793–807. doi: 10.1038/nrn1519

McGarry, L. M., Packer, A. M., Fino, E., Nikolenko, V., Sippy, T., and Yuste, R. (2010). Quantitative classification of somatostatin-positive neocortical interneurons identifies three interneuron subtypes. *Front. Neural Circ.* 4:12. doi: 10.3389/fncir.2010.00012

Mechawar, N., Cozzari, C., and Descarries, L. (2000). Cholinergic innervation in adult rat cerebral cortex: a quantitative immunocytochemical description. *J. Comp. Neurol.* 428, 305–318. doi: 10.1002/1096-9861(20001211)428:2<305::AID-CNE9>3.0.CO;2-Y

Mountcastle, V. B. (1997). The columnar organization of the neocortex. *Brain* 120, 701–722. doi: 10.1093/brain/120.4.701

Munoz, W., Tremblay, R., Levenstein, D., and Rudy, B. (2017). Layer-specific modulation of neocortical dendritic inhibition during active wakefulness. *Science* 355, 954–958. doi: 10.1126/science.aag2599

Munoz, W., Tremblay, R., and Rudy, B. (2014). Channelrhodopsin-assisted patching: in vivo recording of genetically and morphologically identified neurons throughout the brain. *Cell Rep.* 9, 2304–2316. doi: 10.1016/j.celrep.2014.11.042

Naka, A., and Adesnik, H. (2016). Inhibitory circuits in cortical layer 5. *Front. Neural Circ.* 10:35. doi: 10.3389/fncir.2016.00035

Neske, G. T., Patrick, S. L., and Connors, B. W. (2015). Contributions of diverse excitatory and inhibitory neurons to recurrent network activity in cerebral cortex. *J. Neurosci.* 35, 1089–1105. doi: 10.1523/JNEUROSCI.2279-14.2015

Nigro, M. J., Hashikawa-Yamasaki, Y., and Rudy, B. (2018). Diversity and connectivity of layer 5 somatostatin-expressing interneurons in the mouse barrel cortex. *J. Neurosci.* 38, 1622–1633. doi: 10.1523/JNEUROSCI.2415-17.2017

Nogueira-Campos, A. A., Finamore, D. M., Imbiriba, L. A., Houzel, J. C., and Franca, J. G. (2012). Distribution and morphology of nitrergic neurons across functional domains of the rat primary somatosensory cortex. *Front. Neural Circ.* 6:57. doi: 10.3389/fncir.2012.00057

Oberlaender, M., de Kock, C. P. J., Bruno, R. M., Ramirez, A., Meyer, H. S., Dercksen, V. J., et al. (2012). Cell type-specific three-dimensional structure of thalamocortical circuits in a column of rat vibrissal cortex. *Cereb. Cortex* 22, 2375–2391. doi: 10.1093/cercor/bhr317

Oliva, A. A., Jiang, M. H., Lam, T., Smith, K. L., and Swann, J. W. (2000). Novel hippocampal interneuronal subtypes identified using transgenic mice that express green fluorescent protein in GABAergic interneurons. *J. Neurosci.* 20, 3354–3368. doi: 10.1523/JNEUROSCI.20-09-03354.2000

Pfeffer, C. K., Xue, M. S., He, M., Huang, Z. J., and Scanziani, M. (2013). Inhibition of inhibition in visual cortex: the logic of connections between molecularly distinct interneurons. *Nat. Neurosci.* 16, 1068–U130. doi: 10.1038/nn.3446

Pi, H. J., Hangya, B., Kvitsiani, D., Sanders, J. I., Huang, Z. J., and Kepecs, A. (2013). Cortical interneurons that specialize in disinhibitory control. *Nature* 503, 521–524. doi: 10.1038/nature12676

Pohlkamp, T., David, C., Cauli, B., Gallopin, T., Bouche, E., Karagiannis, A., et al. (2014). Characterization and distribution of reelin-positive interneuron subtypes in the rat barrel cortex. *Cereb. Cortex* 24, 3046–3058. doi: 10.1093/cercor/bht161

Porter, J. T., Johnson, C. K., and Agmon, A. (2001). Diverse types of interneurons generate thalamus-evoked feedforward inhibition in the mouse barrel cortex. *J. Neurosci.* 21, 2699–2710. doi: 10.1523/JNEUROSCI.21-08-02699.2001

Prönneke, A., Scheuer, B., Wagener, R. J., Möck, M., Witte, M., and Staiger, J. F. (2015). Characterizing VIP neurons in the barrel cortex of VIPcre/tdTomato mice reveals layer-specific differences. *Cereb. Cortex* 25, 4854–4868. doi: 10.1093/cercor/bhv202

Ren, J. Q., Aika, Y., Heizmann, C. W., and Kosaka, T. (1992). Quantitative analysis of neurons and glial cells in the rat somatosensory cortex, with special reference to GABAergic neurons and parvalbumin-containing neurons. *Exp. Brain Res.* 92, 1–14. doi: 10.1007/BF00230378

Rudy, B., Fishell, G., Lee, S., and Hjerling-Leffler, J. (2011). Three groups of interneurons account for nearly 100% of neocortical GABAergic neurons. *Dev. Neurobiol.* 71, 45–61. doi: 10.1002/dneu.20853

Shigematsu, N., Nishi, A., and Fukuda, T. (2018). Gap junctions interconnect different subtypes of parvalbumin-positive interneurons in barrels and septa with connectivity unique to each subtype. *Cereb Cortex* 29, 1414–1429. doi: 10.1093/cercor/bhy038

Somogyi, P., Tamas, G., Lujan, R., and Buhl, E. H. (1998). Salient features of synaptic organisation in the cerebral cortex. *Brain Res. Rev.* 26, 113–135. doi: 10.1016/S0165-0173(97)00061-1

Staiger, J. F., Masanneck, C., Bisler, S., Schleicher, A., Zuschratter, W., and Zilles, K. (2002). Excitatory and inhibitory neurons express c-Fos in barrel-related columns after exploration of a novel environment. *Neuroscience* 109, 687–699. doi: 10.1016/S0306-4522(01)00501-2

Staiger, J. F., Zilles, K., and Freund, T. F. (1996a). Distribution of GABAergic elements postsynaptic to ventroposteromedial thalamic projections in layer IV of rat barrel cortex. *Eur. J. Neurosci.* 8, 2273–2285. doi: 10.1111/j.1460-9568.1996.tb01191.x

Staiger, J. F., Zilles, K., and Freund, T. F. (1996b). Innervation of VIP-immunoreactive neurons by the ventroposteromedial thalamic nucleus in the barrel cortex of the rat. *J. Comp. Neurol.* 367, 194–204. doi: 10.1002/(SICI)1096-9861(19960401)367:2<194::AID-CNE3>3.0.CO;2-0

Staiger, J. F., Zuschratter, W., Luhmann, H. J., and Schubert, D. (2009). Local circuits targeting parvalbumin-containing interneurons in layer IV of rat barrel cortex. *Brain Struct. Funct.* 214, 1–13. doi: 10.1007/s00429-009-0225-5

Staiger, J. F., Möck, M., Proenneke, A., and Witte, M. (2015). What types of neocortical GABAergic neurons do really exist? *e-Neuroforum* 6, 49–56.

Sukhov, A. G., Kirichenko, E., and Belichenko, L. A. (2016). Structural characteristics and spatial organization of parvalbumin-containing neurons in somatosensory zone SI of the cerebral cortex in rats. *Neurosci. Behav. Physiol.* 46, 863–867. doi: 10.1007/s11055-016-0323-9

Tamas, G., Buhl, E. H., Lorincz, A., and Somogyi, P. (2000). Proximally targeted GABAergic synapses and gap junctions synchronize cortical interneurons. *Nat. Neurosci.* 3, 366–371. doi: 10.1038/73936

Taniguchi, H., He, M., Wu, P., Kim, S., Paik, R., Sugino, K., et al. (2011). A resource of cre driver lines for genetic targeting of GABAergic neurons in cerebral cortex. *Neuron* 71, 995–1013. doi: 10.1016/j.neuron.2011.07.026

Tremblay, R., Lee, S., and Rudy, B. (2016). GABAergic interneurons in the neocortex: from cellular properties to circuits. *Neuron* 91, 260–292. doi: 10.1016/j.neuron.2016.06.033

Urban-Ciecko, J., and Barth, A. L. (2016). Somatostatin-expressing neurons in cortical networks. *Nat. Rev. Neurosci.* 17, 401–409. doi: 10.1038/nrn.2016.53

van Brederode, J. F. M., Helliesen, M. K., and Hendrickson, A. E. (1991). Distribution of the calcium-binding proteins parvalbumin and calbindin-D28k in the sensorimotor cortex of the rat. *Neuroscience* 44, 157–171. doi: 10.1016/0306-4522(91)90258-P

Wagener, R. J., David, C., Zhao, S., Haas, C. A., and Staiger, J. F. (2010). The somatosensory cortex of reeler mutant mice shows absent layering but intact formation and behavioral activation of columnar somatotopic maps. *J. Neurosci.* 30, 15700–15709. doi: 10.1523/JNEUROSCI.3707-10.2010

Wagener, R. J., Witte, M., Guy, J., Mingo-Moreno, N., Kugler, S., and Staiger, J. F. (2016). Thalamocortical connections drive intracortical activation of functional columns in the mislaminated reeler somatosensory cortex. *Cereb. Cortex* 26, 820–837.

Walker, F., Möck, M., Feyerabend, M., Guy, J., Wagener, R. J., Schubert, D., et al. (2016). Parvalbumin- and vasoactive intestinal polypeptide-expressing neocortical interneurons impose differential inhibition on martinotti cells. *Nat. Commun.* 7:13664. doi: 10.1038/ncomms13664

Wall, N. R., De La Parra, M., Sorokin, J. M., Taniguchi, H., Huang, Z. J., and Callaway, E. M. (2016). Brain-wide maps of synaptic input to cortical interneurons. *J. Neurosci.* 36, 4000–4009. doi: 10.1523/JNEUROSCI.3967-15.2016

Wang, Y., Gupta, A., Toledo-Rodriguez, M., Wu, C. Z., and Markram, H. (2002). Anatomical, physiological, molecular and circuit properties of nest basket cells in the developing somatosensory cortex. *Cereb. Cortex* 12, 395–410. doi: 10.1093/cercor/12.4.395

Welker, C., and Woolsey, T. A. (1974). Structure of layer IV in the somatosensory neocortex of the rat: description and comparison with the mouse. *J. Comp. Neurol.* 158, 437–454. doi: 10.1002/cne.901580405

Wimmer, V. C., Broser, P. J., Kuner, T., and Bruno, R. M. (2010a). Experience-induced plasticity of thalamocortical axons in both juveniles and adults. *J. Comp. Neurol.* 518, 4629–4648. doi: 10.1002/cne.22483

Wimmer, V. C., Bruno, R. M., de Kock, C. P. J., Kuner, T., and Sakmann, B. (2010b). Dimensions of a projection column and architecture of VPM and POm axons in rat vibrissal cortex. *Cereb. Cortex* 20, 2265–2276. doi: 10.1093/cercor/bhq068

Woolsey, T. A., and van der Loos, H. (1970). The structural organization of layer IV in the somatosensory region (SI) of mouse cerebral cortex. *Brain Res.* 17, 205–242. doi: 10.1016/0006-8993(70)90079-X

Xu, H., Jeong, H. Y., Tremblay, R., and Rudy, B. (2013). Neocortical somatostatin-expressing GABAergic interneurons disinhibit the thalamorecipient layer 4. *Neuron* 77, 155–167. doi: 10.1016/j.neuron.2012.11.004

Xu, X. M., Roby, K. D., and Callaway, E. M. (2010). Immunochemical characterization of inhibitory mouse cortical neurons: three chemically distinct classes of inhibitory cells. *J. Comp. Neurol.* 518, 389–404. doi: 10.1002/cne.22229

Yavorska, I., and Wehr, M. (2016). Somatostatin-expressing inhibitory interneurons in cortical circuits. *Front. Neural Circ.* 10:76. doi: 10.3389/fncir.2016.00076

Yu, J., Gutnisky, D. A., Hires, S. A., and Svoboda, K. (2016). Layer 4 fast-spiking interneurons filter thalamocortical signals during active somatosensation. *Nat. Neurosci.* 19, 1647–1657. doi: 10.1038/nn.4412

Zembrzycki, A., Chou, S. J., Ashery-Padan, R., Stoykova, A., and O'Leary, D. D. M. (2013). Sensory cortex limits cortical maps and drives top-down plasticity in thalamocortical circuits. *Nat. Neurosci.* 16, 1060–U118. doi: 10.1038/nn.3454

Zhou, X. J., Rickmann, M., Hafner, G., and Staiger, J. F. (2017). Subcellular targeting of VIP boutons in mouse barrel cortex is layer-dependent and not restricted to interneurons. *Cereb. Cortex* 27, 5353–5368. doi: 10.1093/cercor/bhx220

Zilles, K., Hajós, F., Csillag, A., Kalman, M., Sotonyi, P., and Schleicher, A. (1993). Vasoactive intestinal polypeptide immunoreactive structures in the mouse barrel field. *Brain Res.* 618, 149–154. doi: 10.1016/0006-8993(93)90438-S

Conflict of Interest Statement: The authors declare that the research was conducted in the absence of any commercial or financial relationships that could be construed as a potential conflict of interest.